Emine Kaya Ekinci* and Nuray Oktar

Production of value-added chemicals from esterification of waste glycerol over MCM-41 supported catalysts

https://doi.org/10.1515/gps-2018-0034
Received January 25, 2018; accepted May 29, 2018; previously published online October 25, 2018

Abstract: A series of active and selective MCM-41 supported catalysts have been successfully prepared and used for bio-derived glycerol esterification with acetic acid to produce fuel additives. In the synthesis of MCM-41, an acidic hydrothermal synthesis route was used, and silicotungstic acid (STA) and zirconia (ZrO_2) were added to the catalyst structure by wet impregnation. X-ray diffraction, nitrogen adsorption-desorption methods, scanning electron microscopy with energy-dispersive spectroscopy, and inductively coupled plasma-mass spectrometry analysis were used for characterizations of the catalysts. Diffuse reflectance infrared Fourier transform spectroscopy analyses of pyridine-adsorbed catalysts owns Lewis and Brønsted acidity hosting in one, which promotes the esterification reaction of glycerol into glycerol esters with high selectivity. Esterification of glycerol reactions were performed at temperature intervals of 105°C–200°C, with an amount of catalyst equal to 0.5 g, and glycerol/acetic acid molar ratio of 1:6 in a stirred autoclave reactor operated batchwise. STA and ZrO_2-impregnated MCM-41 catalysts showed better performance with a complete glycerol conversion and high selectivity to triacetin.

Keywords: esterification; glycerol; heteropolyacid; MCM-41; zirconia.

1 Introduction

Biodiesel is a renewable clean energy produced by the transesterification of vegetable oils with methanol or ethanol in the presence of alkaline catalyst [1]. It has received much attention due to the growing demand for energy and its benefits for the environment. One of the major drawbacks of the biodiesel industry is the production of large amounts of glycerol. Esterification of glycerol with acetic acid is a good alternative for transforming the residual glycerol to high value-added products. Mono, di, and triacetyl glycerol (MAG, DAG, and TAG, respectively) are the main products obtained in glycerol esterification. The reaction pathway is given in Scheme 1. The acetylated derivatives of glycerol are valuable chemicals that have great industrial applications. The monoacetins are used as a food additives and smokeless powder in the manufacture of explosives [2]. They are also valuable chemicals in the pharmaceutical chemistry [3]. Diacetin has been used as an intermediate in the synthesis of structural lipids, as a plasticizer coating, and also has applications in the food industry as well as in fuel additives [3–5]. The mixture of monoacetin and diacetin has applications in cryogenics and biodegradable polyesters, and it is used as a chemical product in the food and cosmetics industries [6–8]. Triacetin is used as a fuel additive for increasing the octane number in gasoline [9]. In addition, it has applications in cigarette filters and gelatinizing agents. Mixtures of these valuable glycerol derivatives (mono-, di-, and triacetins) have applications as solvents for printing ink and dye stuffs, such as plasticizers and as softening agents [2].

Esterification reactions can be performed in the presence of both homogenous and heterogeneous acid catalysts. Although homogeneous catalysts are widely used in industry for economic reasons, ecological factors favor the use of heterogeneous catalysts. Being noncorrosive and easy to separate from the reaction mixture, heterogeneous catalysts are more preferable in these reactions [10].

There are only a few studies dealing with the esterification of glycerol with acetic acid. A variety of catalysts such as heteropolyacids (HPA) immobilized zeolites, ion exchange resins, and niobic acid have been used in esterification reactions [10–15]. Our previous study was about the esterification of glycerol with acetic acid over ion exchange resins: Amberlyst-15, Amberlyst-16, Amberlyst-36, Amberlite IR-120, and Relite EXC8D [11]. Previous studies showed that the change in product selectivity is attributed to reaction temperature, reaction time, and glycerol to acetic acid molar ratio [11]. In esterification reactions, catalytic activity of acidic ion-exchange resins is quite high. However,

***Corresponding author: Emine Kaya Ekinci,** Department of Chemical Engineering, Gazi University, Maltepe, 06570 Ankara, Turkey, e-mail: eminekaya@gazi.edu.tr. https://orcid.org/0000-0002-0958-1513
Nuray Oktar: Department of Chemical Engineering, Gazi University, Maltepe, 06570 Ankara, Turkey

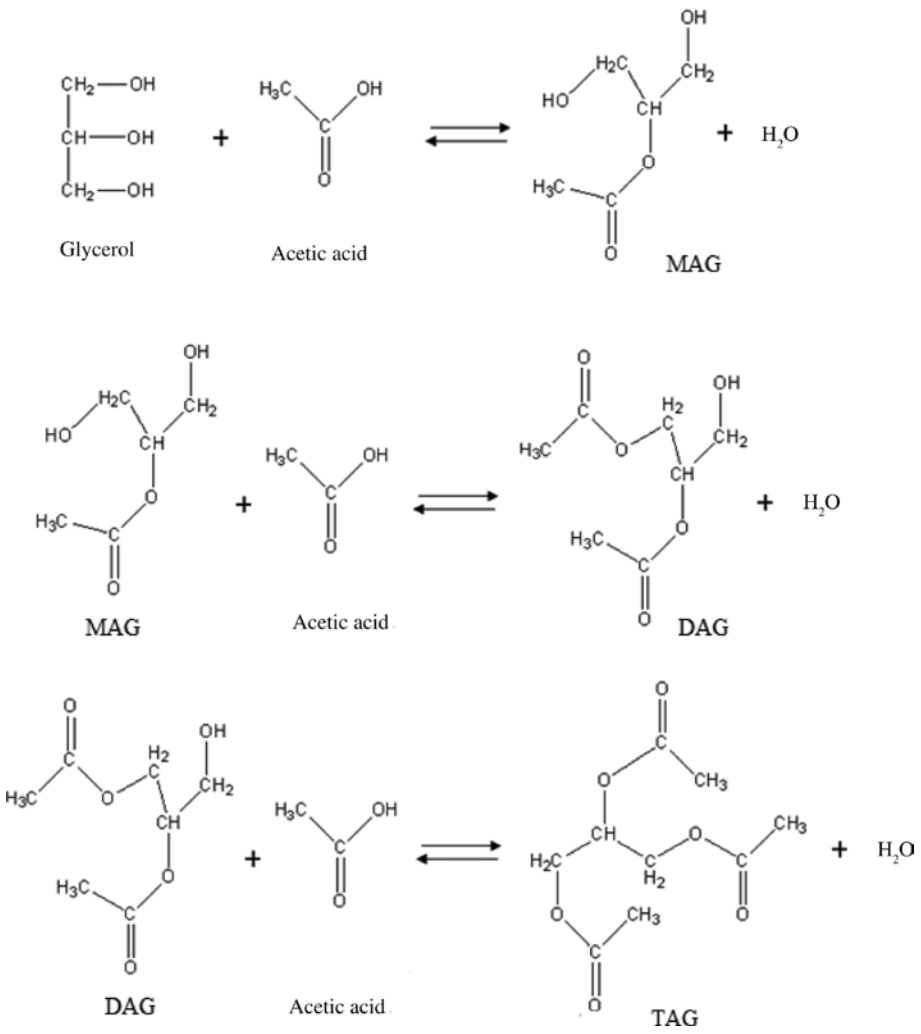

Scheme 1: Glycerol-acetic acid esterification reaction pathway.

they have a very low operating temperature. Because temperature is an important parameter for the rate of reaction, thermal stability is an important parameter for the proper selection of catalyst. Using ordered mesoporous silica, MCM-41, as a catalyst support, offers high thermal stability in catalyst synthesis. Catalytic function to the support is achieved by incorporation of active sites in the silica walls or deposition of active species on the inner surface of the material. The advantages of using ordered mesoporous solids as catalyst support are the relatively large pores facilitating mass transfer and very high surface area allowing a high concentration of active sites per mass of material [16]. Recently, MCM-41 has been studied in the esterification of glycerol with fatty acids such as lauric and oleic acids [17, 18], as well as in the etherification of glycerol to polyglycerols [19]. In the present study, esterification of glycerol with acetic acid was studied over the MCM-41 supported catalyst. MCM-41 shows weak acidity. Various metal oxides and metal ions such as zirconia (ZrO_2), vanadium, iron, and others, can be substituted into the MCM-41 for enhancing catalytic activity [20]. In the present study, zirconia was selected for enhancing the acidity and stability of MCM-41. The synthesized catalysts were characterized and used in glycerol esterification reaction with acetic acid.

It is known that Brønsted acidity has an important role in catalyst activity in esterification reactions [21]. HPA are typically strong Brønsted acids and catalyze a wide variety of reactions in both homogeneous and heterogeneous phases [14]. However, HPAs have some disadvantages such as low surface area, low thermal stability, and solubility in polar media. Supporting HPAs on mesoporous support such as MCM-41 provides large surface area, higher thermal stability and insolubility in reaction medium. To catalyze the esterification of glycerol with acetic acid, silicotungstic acid (STA) incorporated ZrO_2-MCM-41 (STA-ZrO_2-MCM-41) catalyst were successfully prepared and characterized. Its

activity was compared with ZrO_2-MCM-41 in the esterification of glycerol with acetic acid. Reactions were performed at temperature intervals of 105°C–200°C in a batch reactor. MCM-41 based catalysts have higher thermal stability compared with acidic resins. Regarding the esterification reactions of glycerol, this work is important for catalyst synthesis with higher triacetin selectivity.

2 Materials and methods

2.1 Catalyst preparation

MCM-41 was synthesized following the acidic route using the hydrothermal synthesis method, and STA and zirconia (ZrO_2) were added to the catalyst structure by wet impregnation. The hydrothermal procedure used in MCM-41 synthesis was described in our previous publication [22]. Conventionally, hydrothermal synthesis of MCM-41 is carried out in a basic medium at a pH of approximately 11; however, in the present study, MCM-41 was synthesized using an acidic direct hydrothermal synthesis route. In this procedure, hexadecyltrimethylammonium bromide (CTMABr, 99% pure; Merck) was used as a surfactant, and tetraethylortosilicate (TEOS, 99% pure; Merck) was used as a silica source. Surfactant solution was prepared by continuous mixing of 13.2 g of CTMABr in 87 ml of deionized water at 30°C. Then, a solution of tetraethylortosilicate was slowly added to this mixture under continuous stirring. The pH of the solution was adjusted (~1.6) and the produced gel was transferred into a Teflon-lined autoclave for hydrothermal synthesis at 120°C for 96 h. The solid product was filtered and then washed until the pH of the wash liquid was almost neutral. The solid material was then dried under vacuum and calcined in a flow of dry air. During calcination, the furnace temperature was increased at a rate of 1°C/min until 550°C, and then calcination was continued at this temperature for 6 h. ZrO_2 and STA were impregnated into MCM-41 supports using an incipient wetness impregnation method. The impregnated amounts for both ZrO_2 and STA were determined according to the literature [21]. In the first set of experiments, ZrO_2/MCM41 catalysts were prepared. An appropriate amount of $ZrO(NO_3)_2.\times H_2O$ (zirconium(IV) oxynitrate hydrate) (99% pure; Sigma Aldrich) was dissolved in deionized water to obtain 20% (w/w) ZrO_2 over MCM-41 samples. The resulting mixture was stirred at 80°C in a magnetic stirrer for 2–3 h. After impregnation, samples were typically dried at 110°C overnight and the calcination procedure was repeated.

STA-ZrO_2-MCM-41 catalyst was prepared by following the same procedure. An appropriate amount of $H_4[SiO_4(W_3O_9)_4]\times H_2O$ (STA hydrate) (Sigma Aldrich, St Louis, MO, USA) was used to obtain 15% STA (w/w) over ZrO_2/MCM41. Then, samples were typically dried at 110°C overnight and the calcination procedure was repeated. However, STA-ZrO_2-MCM-41 catalyst was calcined at 300°C due to the low thermal stability of STA [23].

2.2 Catalyst characterization

The X-ray diffraction (XRD) patterns of MCM-41 supported catalysts were obtained using Bruker/D8 Advance diffractometer with CuKα radiation ($\lambda = 1.5418$ Å), and scintillation detector. Diffraction patterns were recorded at steps of 0.01°/s. The phase composition was determined by comparing measured *d*-spacing values. All measurements were made at room temperature.

The BET surface area values and pore size of the catalysts were determined by nitrogen adsorption-desorption experiments (Quantachrome Corporation, Autosorb-1-C/MS). Pore size distributions and pore diameter were calculated using the Barret-Joyner-Halenda (BJH) method.

Surface morphology and elemental composition on the surfaces of the catalysts were determined by a scanning electron microscopy with energy-dispersive spectroscopy (SEM-EDS; QUANTA 400F Field Emission). The composition of silica, zirconium, and tungsten were measured using inductively coupled plasma-mass spectrometry (ICP-MS; Perkin Elmer DRC II).

The Fourier transform infrared (FTIR) spectrum of catalyst before reaction and after reaction were determined. To determine the Lewis or Brønsted acidic sites of the catalysts, the samples were initially treated with pyridine and then analyzed using diffuse reflectance (diffuse reflectance infrared Fourier transform spectroscopy or DRIFTS). Experiments were conducted on a Perkin Elmer instrument in the range of 380–4000 cm^{-1}.

2.3 Esterification and activity measurements

Reaction studies were performed at identical conditions. A 0.5 g catalyst loading, which corresponded to 0.9 wt% of the total reaction mixture, was used in reactions and experiments were performed with a 1:6 glycerol/acetic acid molar ratio. The reaction system was composed of an autoclave operated autogenously with a magnetic stirrer. The reaction temperature was controlled with ±1°C precision in the course of experiments. The effect of the reaction temperature on glycerol conversion and product selectivity was investigated at temperature intervals of 105°C–200°C. To monitor the reaction, samples were withdrawn periodically at different time intervals and analyzed by gas chromatography (Agilent 6890 N) equipped with HP Innowax column and a flame ionization detector. The conversion of the glycerol and the selectivities were calculated as follows:

$$\%\ \text{Conversion of glycerol} = (\text{number of glycerol moles reacted}/\text{total number of moles of glycerol in the feed}) \times 100$$

$$\%\ \text{Selectivity} = (\text{number of moles of desired product}/\text{number of glycerol moles reacted}) \times 100$$

Reaction studies were carried out three times for the reproducibility of conversion data.

3 Results and discussion

3.1 Catalyst characterization results

The XRD patterns of the MCM-41 supported catalysts are shown in Figure 1. MCM-41 was known to have a well-ordered lattice structure with hexagonal unit cell. A limited number of reflections situated at the low angle region is a

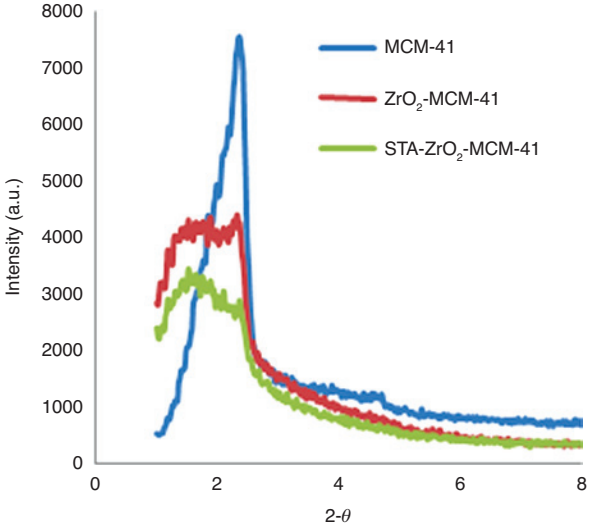

Figure 1: XRD patterns of MCM-41 and MCM-41 supported catalysts.

characteristic of the structure. The sharp Bragg peak corresponding to $d(100)$ was observed at 2θ value of 2.4°. By the impregnation of ZrO_2, a slight decrease was observed in characteristic Bragg peak. The XRD patterns of ZrO_2 and STA impregnated catalysts showed much wider $d(100)$ values than the corresponding peak observed for pure MCM-41. The wide band corresponds to wide distribution of pore sizes [24].

The nitrogen adsorption-desorption isotherms of the MCM-41 supported catalysts exhibited typical type IV isotherms according to International Union of Pure and Applied Chemistry classification and revealed the hysteresis effect as shown in Figure 2. The surface area of the pure MCM-41 that was synthesized using the acidic route hydrothermal synthesis was 760 m^2/g. By the impregnation of ZrO_2 and STA, the surface area was decreased to 502 and 358 m^2/g, respectively. Physical properties of the

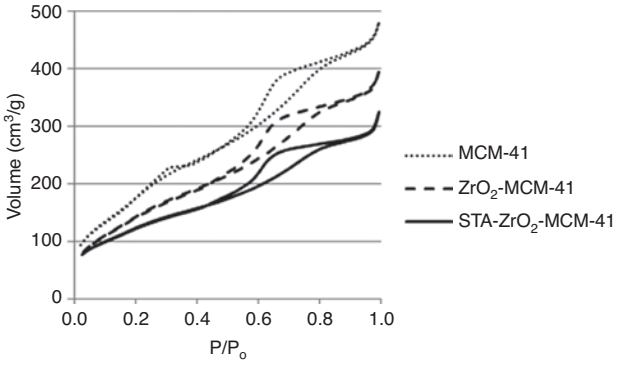

Figure 2: N_2 adsorption-desorption isotherms of MCM-41 supported catalysts.

catalysts are listed in Table 1. The characteristic lattice parameter (the repeating distance "a" between two pore centers) was calculated from the following equation [22]:

$$a = 2d_{(100)}/\sqrt{3} \quad (1)$$

The pore wall thickness δ was then estimated from the average pore diameter (dp) and the lattice parameter (a) [22]:

$$\delta = a - 0.95d_p \quad (2)$$

The average pore diameters of the bare MCM-41 and ZrO_2 and STA-impregnated catalysts were determined by the BJH pore size distributions as 2.7, 2.0, and 1.9 nm, respectively. The pore volume was decreased significantly with the impregnation of ZrO_2 to the silica, which indicates pore filling. However, the pore wall thicknesses also increased due to the impregnation of ZrO_2. Impregnation of ZrO_2 on MCM-41 resulted in the dispersion of zirconia inside the pores that, in our opinion, facilitated the formation of larger wall thickness and improved mechanical strength.

Figure 3 shows the particle morphology of the MCM-41 supported catalyst using the SEM method. ZrO_2 was well-ordered and distributed uniformly on the support surface as seen in Figure 3A. Due to the impregnation method used for the catalyst preparation, agglomeration could be naturally seen on the surface; however, there is no accumulation seen on the support surface. In Figure 3B, the image of STA-ZrO_2-MCM-41 catalyst, the small particles can be clearly seen on the surface. This was due to the presence of STA, which was attached to the mesopores and surface of the catalyst uniformly. Si, Zr, and W contents in the MCM-41 supported catalysts were obtained by SEM-EDS and ICP-MS. Zr and W contents were measured and showed much closer values using both methods given in Table 2. According to the results on SEM-EDS and ICP-MS, ZrO_2 and STA impregnation onto the catalyst structure was successfully conducted.

The acidity of the catalyst plays an effective role in esterification reactions. Therefore, DRIFTS analysis was conducted on the pyridine-adsorbed MCM-41 supported catalysts to determine the Brønsted and Lewis acid sites. In Figure 4, the DRIFT spectrum of pyridine-adsorbed catalysts were given. The peaks between 1540 cm^{-1} and 1640 cm^{-1} validate the presence of Brønsted acid sites [25]. The wide peak at 1630 cm^{-1} became more apparent with the incorporation of STA. Also, a small peak at 1540 cm^{-1} was observed in STA and zirconia impregnated catalysts. Another peak at 1486 cm^{-1}, which revealed the presence of Lewis-Brønsted acid sites, was obtained with these

Table 1: Physical properties of the MCM-41 supported catalysts.

Physical property/catalyst	MCM-41	ZrO_2-MCM-41	STA-ZrO_2-MCM-41
d(100)	3.84	3.68	3.68
Lattice parameter "a" (nm)	4.43	4.25	4.25
Surface area (BET) (m^2/g)	760	502	358
Pore volume (cm^3/g)	0.86	0.67	0.52
Average pore diameter (nm)	2.7	2.0	1.9
Pore wall thickness (nm)	1.9	2.3	2.4

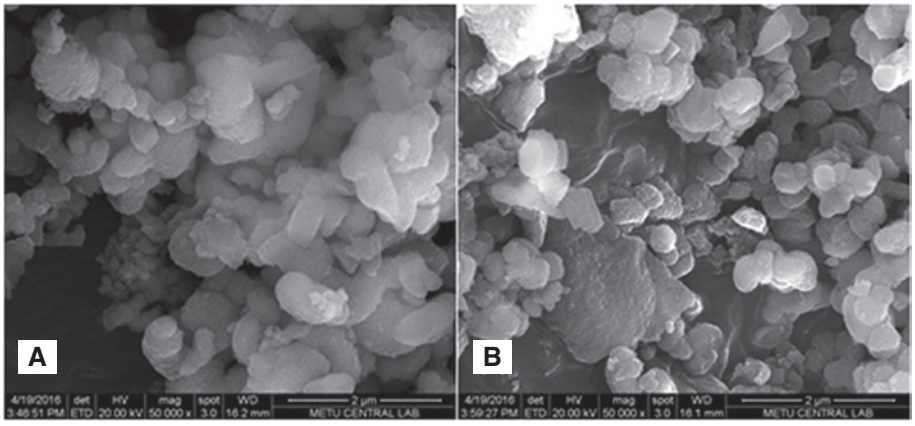

Figure 3: SEM images of MCM-41 supported catalysts (A) ZrO_2-MCM-41, (B) STA-ZrO_2-MCM-41.

Table 2: The elemental analysis data of MCM-41 supported catalysts.

Element %	EDS measurements		ICP-MS measurements	
	ZrO_2-MCM-41	STA-ZrO_2-MCM-41	ZrO_2-MCM-41	STA-ZrO_2-MCM-41
Si	38	38	32	30
Zr	17	8.8	11.5	8.8
W	–	7.8	–	8

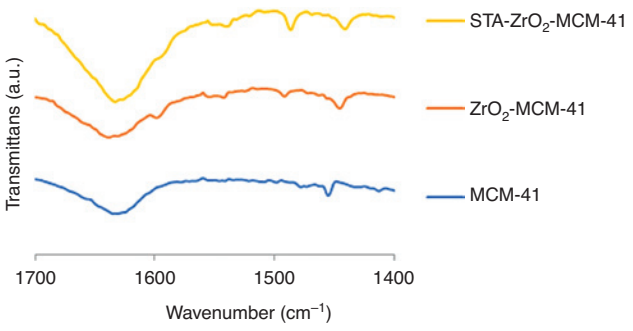

Figure 4: DRIFT spectrum of pyridine-adsorbed catalysts.

catalysts. Finally, the peak obtained at 1440 cm^{-1} validated the presence of Lewis acid sites for all catalysts [25]. According to the DRIFTS analysis of the pyridine-adsorbed catalyst, the impregnation of STA and zirconia increased the acidic sites of the catalysts.

STA is an HPA catalyst that considered to be a highly attractive solid acid catalyst, having superior acidic characteristics. The major disadvantages of STA is its very low surface area, low thermal stability, and solubility in the presence of polar solvents. Supporting STA on mesoporous support such as MCM-41 provides large surface area, higher thermal stability, and insolubility in reaction medium. FTIR analysis of fresh and used catalysts was carried out to understand whether the STA was dissolved in the reaction medium and separated from the support. FTIR analysis of STA-impregnated ZrO_2-MCM-41 catalysts are shown in Figure 5. A series of characteristic peaks were observed between 700 and 1200 cm^{-1} for used and fresh catalysts, respectively. These peaks belonged to the

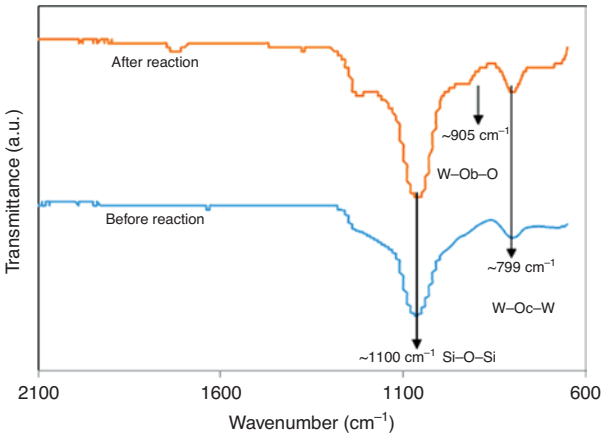

Figure 5: FTIR Spectrum of STA-ZrO_2-MCM-41.

primary structure of $[SiW_{12}O_{40}]^{-4}$ of the catalysts [23]. The typical FTIR bands obtained at 1100 cm^{-1} correspond to Si–O–Si present in the structure of both STA and MCM-41. The peak observed at 799 cm^{-1} showed binding of oxygen and tungsten (W–Oc–W corner shared). In the FTIR analysis of used catalysts, the peak at 905 cm^{-1} belonged to the (W–Ob–W edge sharing) [23]. It was seen from the FTIR spectrum (Figure 5) that STA had essentially retained its molecular structure after the reaction.

3.2 Glycerol esterification results

Esterification of glycerol with acetic acid was conducted in the presence of MCM-41 and MCM-41 supported catalyst at a constant temperature (105°C) and the results are shown in Figure 6. Reaction parameters such as initial reactant ratio (glycerol/acetic acid molar ratio, 1:6), mixing rate (1000 rpm), and catalyst amounts (0.5 g) were determined according to our previous studies in which

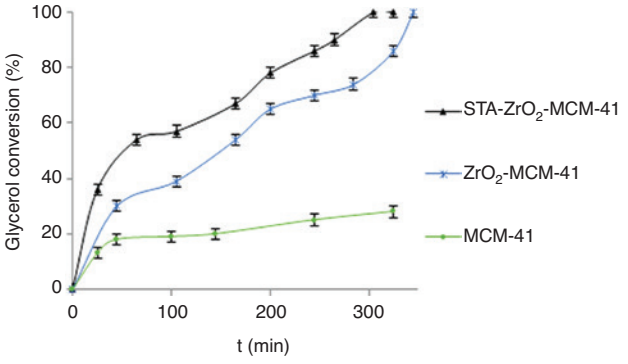

Figure 6: Glycerol conversion of the reactions catalyzed by MCM-41 supported catalysts.

ion exchange resins, such as Amberlyst-15, were used as catalysts [12]. The reaction took place for 345 min and the products were analyzed at different time intervals. After the impregnation of ZrO_2 and STA to MCM-41, the resulting catalyst was seen to be more active at shorter times. The glycerol conversion reached 100% by the end of the 345th minute in the reaction catalyzed by ZrO_2-MCM-41. It was seen that STA impregnation to ZrO_2-MCM-41 had accelerated the reaction, which had reached completion by the end of the 305th minute. Product distributions at the end of the 345th minute were the same for all MCM-41 supported catalysts used in the reactions: 52% MAG, 41% DAG, and 7% TAG selectivity were obtained. Similar to our study, zeolite esterification of glycerol with acetic acid was studied over dodecatungstophosphoric acid immobilized into a silica matrix at 120°C and it was reported that after 7 h of reaction time, the glycerol conversion was 87%, with a selectivity of 59% to diacetin, 36% to monoacetin, and 4% to triacetin [26]. Based on these results, the MCM-41 based catalysts used in this study are obviously active for the esterification reactions.

The presence of Brønsted acid sites in the STA structure plays an important role in the esterification reactions [10]. However, when used as a catalyst, HPAs dissolve in polar mediums after the reaction. In the case of STA-ZrO_2-MCM-41, the characteristic peaks of STA were preserved as indicated in the FTIR spectrum (Figure 5). In other words, STA remained in the catalyst structure after the reaction.

To increase TAG selectivity, reaction experiments were performed in the presence of STA-ZrO_2-MCM-41 at 200°C. The results indicated accelerated reaction by increasing the reaction temperature with completion of glycerol conversion at the end of 245 min. The results are listed in Table 3. In our previous study on esterification of glycerol with acetic acid catalyzed by Amberlyst-15, it took 245 min to reach complete conversion at 105°C [12].

Esterification of glycerol with acetic acid is a consecutive reaction. The enhancement of temperature accelerated further esterification of MAG to form DAG and TAG. As a result of increasing temperature, the selectivity values of DAG and TAG were increased whereas the selectivity value of MAG was decreased. The TAG selectivity increased from 4% to 21%. This selectivity value was higher than the one determined in the presence of Amberlyst-15. In our previous study, it was observed that the activity of Amberlyst-15 had not been stable at temperatures higher than 110°C in acetic acid media because of the temperature constraints. On the other hand, MCM-41 supported catalysts retained their activity until 200°C.

The use of MCM-41 supported catalysts enabled us to accelerate the reaction and control the product

Table 3: Catalytic activities of the catalysts (reaction time, 245 min).

Catalyst	Reaction temperature (°C)	Glycerol conversion (%)	Selectivity (%)		
			MAG	DAG	TAG
Amberlyst-15 [13]	105	100	30	57	13
MCM-41	105	25	34	55	11
ZrO_2-MCM-41	105	70	60	34	6
STA-ZrO_2-MCM-41	105	86	58	38	4
STA-ZrO_2-MCM-41	200	100	37	42	21

distribution by simply changing the reaction temperature. The use of a catalyst with a high temperature stability is very important for such consecutive reactions. The work being undertaken is important in terms of using an alternative catalyst for esterification reactions.

4 Conclusions

The esterification of glycerol with acetic acid can be considered as a good choice for the utilization of glycerol. Liquid phase esterification reaction of glycerol with acetic acid has been studied in the presence of STA and ZrO_2 incorporated mesoporous MCM 41 catalysts. According to the physical characterization tests, the crystal structure of MCM-41 was obtained and high surface areas were achieved at the end of synthesis. The Brønsted acid sites of the catalysts were determined using DRIFTS. Reaction results indicated that glycerol could be successfully esterified with acetic acid in the presence of STA and zirconia incorporated MCM-41 catalysts. STA-ZrO_2-MCM-41 catalyst showed good activity in the esterification reaction providing 100% glycerol conversion and 21% selectivity to the TAG in a reaction time of 245 min at 200°C. Because the glycerol conversion is well correlated with the acidity of the catalysts, STA-impregnated catalysts were more active due to the Brønsted acid sites.

Acknowledgments: The financial support from the Gazi University Research Fund (06/2010-32) is gratefully acknowledged.

References

[1] Özbay N, Oktar N, Tapan NA. *Fuel* 2008, 87, 1789–1798.
[2] Nebel B, Mittelbach M, Uray G. *Anal. Chem.* 2008, 80, 8712–8716.
[3] Sastry SV, Wilber W, Reddy IK, Khan MA. *Int. J. Pharm.* 1998, 165, 175–189.
[4] Watanabe T, Sugiura M, Sato M, Yamada N, Nakanishi K. *Process Biochem.* 2005, 40, 637–643.
[5] Baur FJ *J. Am. Oil Chem. Soc.* 1954, 31, 196–199.
[6] Taguchi Y, Oishi A, Ikeda Y, Fujita K, Masuda T. JP Patent, 298099, 2000.
[7] Lal SND, Connor CJO, Eyres L. *Adv. Colloid Interface Sci.* 2006, 123, 433–437.
[8] Baumann H, Buhler M, Fochem H, Hirsinger F, Zoebelein H, Falbe J. *Angew. Chem. Int. Ed.* 1988, 27, 41–62.
[9] Liao X, Zhu Y, Wanga S-G, Chen H, Li Y. *Appl. Catal. B: Environ.* 2010, 94, 64–70.
[10] Ferreira P, Fonseca IM, Ramos AM, Vital J, Castanheiro JE. *Catal. Commun.* 2009, 10, 481–484.
[11] Ekinci EK, Gündüz G, Oktar N. *J. Fac. Eng. Archit. Gaz.* 2015, 30, 443–450.
[12] Ekinci EK, Gündüz G, Oktar N. *Int. J. Chem. React. Eng.* 2016, 14, 309–314.
[13] Liao X, Zhu Y, Wanga S-G, Chen H, Li Y. *Fuel Process. Tech.* 2009, 90, 988–993.
[14] Balaraju M, Nikhitha P, Jagadeeswaraiah K, Srilatha K, Sai Prasad PS, Lingaiah N. *Fuel Process. Tech.* 2010, 91, 249–253.
[15] Gonçalves LC, Pinto BP, Silva JC, Mota CJA. *Catal. Today* 2008, 133–135, 673–677.
[16] Taguchi A, Schüth F. *Micropor. Mesopor. Mater.* 2005, 77, 1–45.
[17] Nakamura R, Kamura K, Sugi Y. *Catal. Commun.* 2008, 9, 511–515.
[18] Perez-Pariente J, Diaz I, Mohino F, Sastre E. *Appl. Catal. A: Gen.* 2003, 254, 173–188.
[19] Clacens JM, Pouilloux Y, Barrault J. *Appl. Catal. A: Gen.* 2002, 227, 181–190.
[20] Ciesla U, Schüth F. *Micropor. Mesopor. Mater.* 1999, 27, 131–149.
[21] Sawant DP, Vinu A, Justus J, Srinivasu P, Halligudi SB. *J. Mol. Catal. A: Chem.* 2007, 276, 150–157.
[22] Kaya E, Oktar N, Karakas G, Murtezaoglu K. *Turk. J. Chem.* 2010, 34, 935–943.
[23] Degirmenci L, Oktar N, Dogu G. *Fuel Process. Tech.* 2010, 91, 737–742.
[24] Sener C, Dogu T, Dogu G. *Micropor. Mesopor. Mater.* 2006, 94, 89–98.
[25] Tanabe K, Misono M, Ono Y, Hattori H. *Stud. Surf. Sci. Catal.* 1989, 51, 5–25.
[26] Ferreira P, Fonseca IM, Ramos AM, Vital J, Castanheiro JE. *Appl. Catal. B:Environ.* 2009, 91, 416–422.